IOP Publishing Measurement Science and Technology
Meas. Sci. Technol. **31** (2020) 054006 (9pp) https://doi.org/10.1088/1361-6501/ab6ecb

Local geometric error corrections for a metrological scanning probe microscope

Bakir Babic, Victoria A Coleman and Jan Herrmann

National Measurement Institute Australia, 36 Bradfield Road, West Lindfield NSW 2070, Australia

E-mail: bakir.babic@measurement.gov.au

Received 7 November 2019, revised 28 December 2019
Accepted for publication 22 January 2020
Published 6 February 2020

Abstract

A local geometric error correction method is developed for a metrological scanning probe microscope. The method corrects geometric errors in stage displacements using the interferometric measurements of angular position and known geometric offsets. Local and global error correction methods are considered and general scaling dependences on the number of measured steps or points are derived and compared. For the local method, the total uncertainty scales the same or decreases with a sufficient number of measurement steps compared with the global method. Implementation of the local geometric error correction method is demonstrated on measurements of a three-dimensional height standard artefact. The applied error correction method reduces the contribution of geometric errors to the uncertainty budget by two orders of magnitude. The presented approach can be extended to any scanning technique where a measurement translation mechanism can be identified and accurately quantified by relating the measured values with a measurand.

Keywords: scanning probe microscopy, error correction, uncertainty analysis, nanometrology

(Some figures may appear in colour only in the online journal)

1. Introduction

Error correction plays a critical role in fundamental science such as quantum computing [1], all the way to trajectory corrections for spectacular interplanetary journey [2]. In metrology, correcting for errors is useful step in improving accuracy when further minimisation of error contributions is not feasible due to practical or economical limitations. Dimensional nanometrology often faces the formidable challenge of achieving subnanometre accuracy of displacement measurements in a measurement volume of hundreds of cubic micrometres, which would be unattainable without error corrections.

At the National Measurement Institute Australia (NMIA) a metrological scanning probe microscope (mSPM) is developed as the primary standard for dimensional measurements at the nanoscale [3]. The instrument achieves traceability to the International System of Units (SI) by interferometric measurement, using a frequency stabilised laser, of the displacement of a sample translation stage, relative to a fixed tip mounted on a quartz tuning fork. The three-dimensional (3D) motion of the nano-positioning stage is measured by five interferometers, one for each of the three translational axes and two for monitoring stage rotations [4]. Geometric errors, such as Abbé errors, cosine errors and other alignment errors contribute to the uncertainty of the displacement measurements. These errors are reduced through the system design and with appropriate alignment procedures. The alignment procedure for estimating and minimising the Abbé off-sets of a multiple beam interferometer is a complex task [5] and will be described elsewhere. A simple estimate taking into account the sample stage's parasitic rotations with known Abbé off-sets shows that the Abbé errors are the largest cumulative contributions to the uncertainty budget of the instrument for displacements above 1 µm. For the mSPM's total in-plane scan range of 100 µm × 100 µm in x and y directions, the Abbé errors comprise $\approx 77\%$ of the uncertainty budget in the z direction. It is therefore desirable to consider application of error correction methods to reduce the geometric errors in the mSPM.

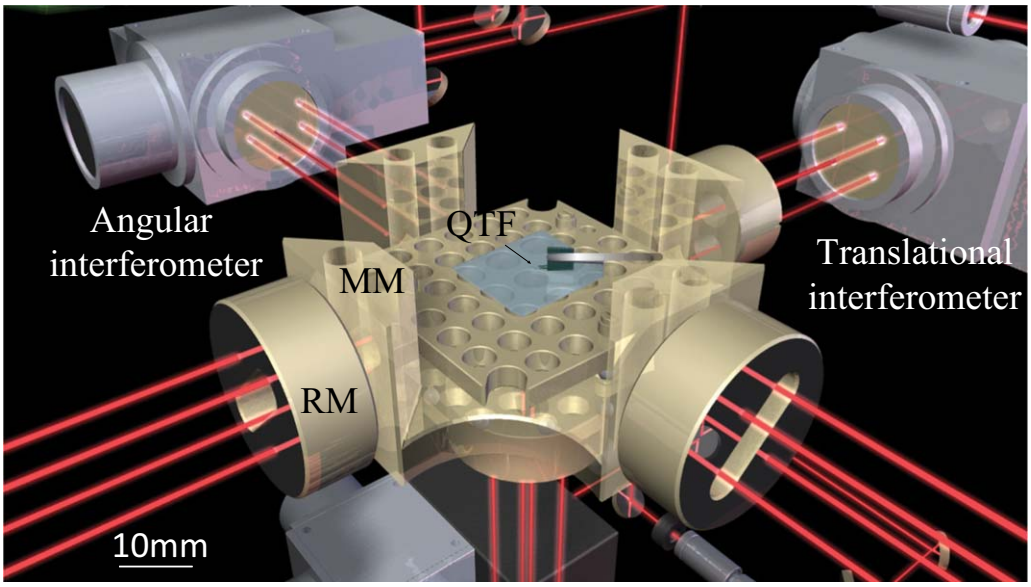

Figure 1. Layout of the measurement set-up in the mSPM. RM—reference mirror, MM—movable mirror, QTF—quartz tuning fork. The TRS origin is located at the QTF's apex whereas the MRS origin is located at the virtual intersection of the extrapolated geometric mean of the interferometric beams.

Here, we present a local geometrical error correction (GEC) method with its implementation demonstrated on a typical dimensional measurement taken with the mSPM. We assume an ideally rigid mirror where, for example, thermal and other contributions to the geometric errors, such as dynamic or software corrections [6] are not considered as they are found to lead to an order of magnitude smaller contributions to the geometric errors for a typical mSPM measurement, compared to the alignment error contributions.

2. Geometric errors

The displacement and change of orientation of a 3D–body, such as a scanning stage with respect to a fixed probe tip, can be specified by measurements of three translations and three rotations. For the mSPM, we consider two distinct reference systems: the true reference system (TRS) relates to the true displacement of the stage with respect to the tip, and the measurement reference system (MRS) whose origin is defined as the interferometric beam intersection[1]. In figure 1, a portion of the mSPM measurement system is graphically represented showing the complexity of measurement translation mechanism between the TRS and MRS. A displacement between these two reference systems represents the Abbé offset between the tip and the interferometer (TIO). In addition, the measurement position in the MRS is offset from the TRS by I_x, I_y and I_z in the x, y and z directions, respectively. These offsets combined with unwanted rotations of the stage, introduce geometric errors result in measurement errors. For small (< 10 µrad) stage rotations, the geometric errors are well approximated by simply multiplying the offsets and the parasitic rotations. If all the offsets are known and the parasitic rotations are measured, the geometric errors can be determined and corrected for. After a correction is applied, the contribution of the geometric errors to the uncertainty budget is estimated from the standard error propagation calculation [7] for individual geometric error components x_i:

$$\Delta g = \sqrt{\sum_{i=1}^{n} \left(\frac{\partial g_i}{\partial x_i}\right)^2 \Delta x_i^2}, \tag{1}$$

where Δg represents the uncertainty of the geometric error g, Δx_i represents the uncertainty of x_i, and $\frac{\partial g_i}{\partial x_i}$ is the sensitivity coefficient for the ith independent geometric error variable.

2.1. 2D geometric errors

Let us consider an exaggerated two-dimensional (2D) movement of a mirror as in figure 2 and identify a geometric relation amongst the parameters of interest. Here, yaw and roll rotation[2], as well as z-axis movement, are set to 0. Only pitch rotations and x and y translations are considered. The initial mirror position is parallel to the x and y translation axes, with no rotation of the mirror. Here, the movement in x direction is C_X, the movement in y direction is C_Y, the rotation of the mirror is β, and the Abbé offsets are A_X and A_Y. The initial mirror orientation and position define the reference coordinate system (x, y). The corner of the mirror defines the origin O. This simplifies the relationships between the geometric parameters. From figure 2, relationships can be established between

[1] In the rest of the text we will assume that each interferometer contains a single beam although in practice each interferometer contains at least four beams. Nevertheless, the applied analysis is valid since the single beam can be considered as the geometric mean of the multiple interferometric beams.

[2] In the article yaw, pitch and roll angles are defined with respect to the x–axis displacement.

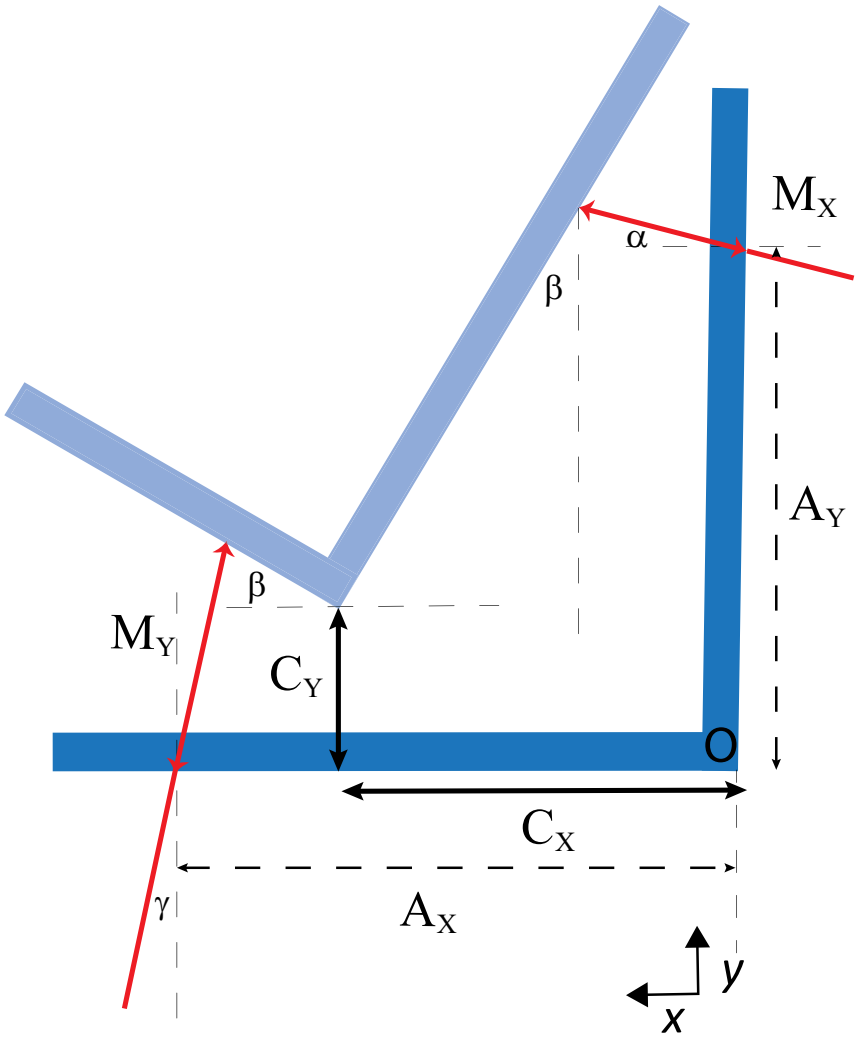

Figure 2. Exaggerated displacement of the mirror in x and y directions while rotating by angle β. The interferometric distance measurements are M_X, M_Y, the probe offsets A_X, A_Y, the mirror's origin movement C_X, C_Y in the x and y directions, respectively. The interferometer beams are incident to the mirror at an angle α for x, and γ for y directions.

the interferometric displacement measurements M_X, M_Y, and the mirror displacements C_X, C_Y. The following equations are found for the mirror displacement in x and y directions expressed via the measurable quantities $M_X, M_Y, A_X, A_Y, \beta$:

$$\begin{aligned} C_X &= \cos^2(\beta)\left[M_X + \tan(\beta)[A_Y - M_Y + A_X \tan(\beta)]\right] \\ C_Y &= \cos^2(\beta)\left[M_Y + \tan(\beta)[-A_X + M_X + A_Y \tan(\beta)]\right]. \end{aligned} \tag{2}$$

If the mirror is not aligned perpendicular to the interferometer beams, cosine errors are introduced determined by the angles between mirror normals and beams. These angles are labeled α and γ in figure 2 and lead to additional corrections in equation 2. Also, when the initial mirror orientation has a non-zero rotation θ, with respect to the translation axes, the true displacements T_X, T_Y are obtained by multiplication with the 2D rotation matrix:

$$\begin{pmatrix} T_X \\ T_Y \end{pmatrix} = \begin{pmatrix} \cos(\theta) & -\sin(\theta) \\ \sin(\theta) & \cos(\theta) \end{pmatrix} \cdot \begin{pmatrix} C_X \\ C_Y \end{pmatrix}. \tag{3}$$

This angle just adds to the incident angles of the interferometer beams. Since the cosine error is of second order for small angles and to capture the notation in more transparent way, in the rest of the paper the beams are assumed incident perpendicular to the mirror which is rotated by an initial angle θ. The initial mirror rotation together with accumulated mirror, i.e. $\alpha = \gamma = 0$, displacements lead to the corrected offsets:

$$\begin{aligned} A_X &= \frac{I_x + TIO_x + \sum T_X}{\cos(\theta)}, \\ A_Y &= \frac{I_y + TIO_y + \sum T_Y}{\cos(\theta)}. \end{aligned} \tag{4}$$

Now that the movement of the mirror corner is obtained, we can derive the movement of a general point on the mirror. This is necessary due to the fact that the pivot point for the mirror rotation, as experimentally deduced, is not at the mirror corners or surfaces, but rather at the fixed tip position. A general approach requires transformations of a point on the mirror by a translation and a rotation about an arbitrary pivot point

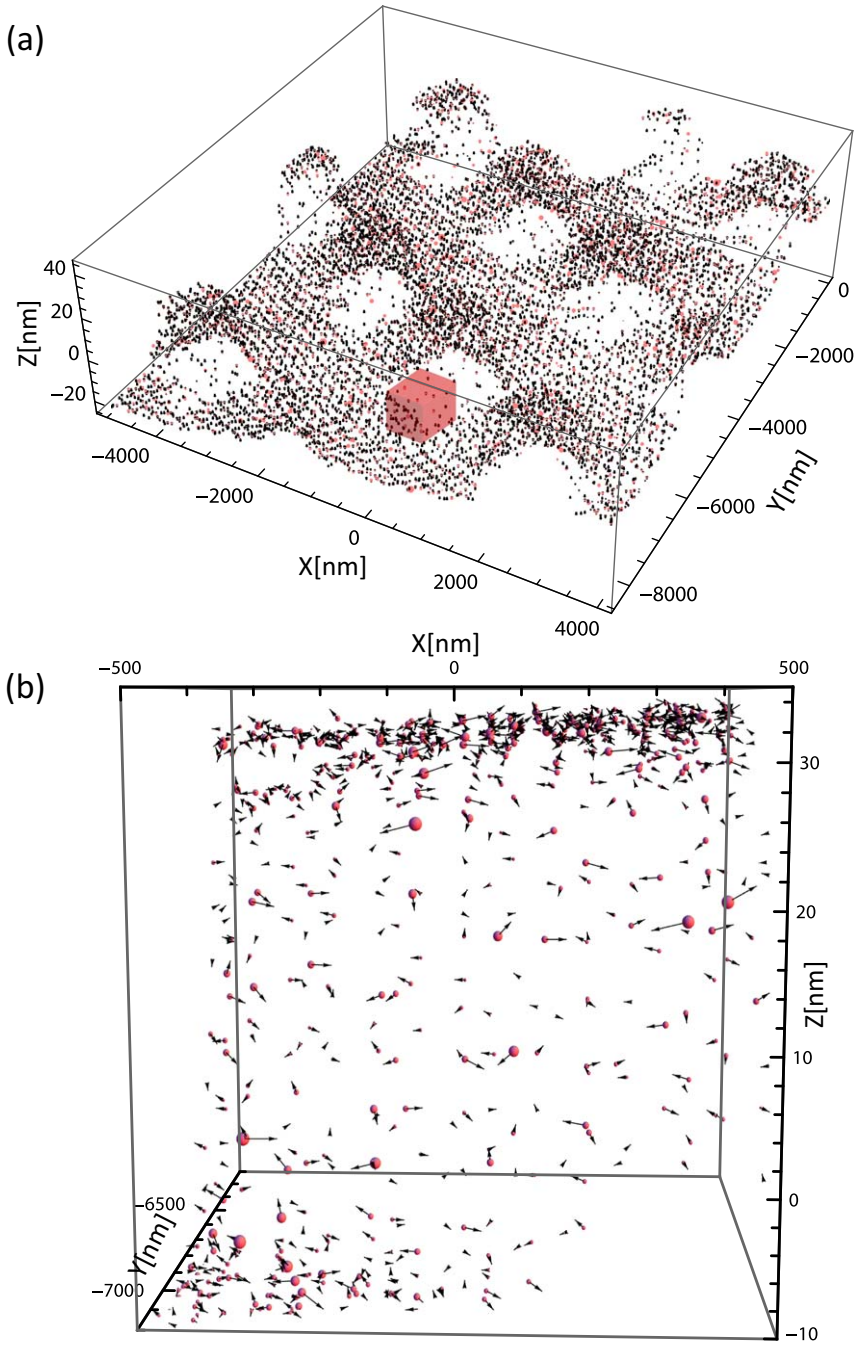

Figure 3. (a) Local correction vectors (black) and their corresponding uncertainties visualised as spheres (red) with the norm of x, y, z uncertainties as their diameters. The mean of the correction vector norms is 0.65 nm and the maximum local uncertainty is 0.22 nm. Every 364th point is shown from the acquired data set. (b) 3D plot of the zoomed in region indicated by the red cube in (a). The local correction vectors are enlarged 40, 40, 2 times while corresponding uncertainties 80, 80, 4 times in the x, y, z directions, respectively. Every 50th point is shown from the acquired data set.

between different coordinate systems. These affine transformations expressed in homogeneous coordinates [8] enable the translations and rotation to be concatenated when written in matrix form. To rotate a displacement about the pivot point, the existing displacement is translated to the pivot point, rotated around the pivot point, and then translated back by the negative of the initial translation to the pivot point. The complete movement can be expressed:

$$Movement = Displacement \cdot ToPivot \cdot Rotation \cdot FromPivot.$$

If (V_X, V_Y) are the coordinates of the pivot point, the movement written explicitly in the matrix form has the following form:

$$\boldsymbol{M} = \begin{pmatrix} 1 & 0 & T_X \\ 0 & 1 & T_Y \\ 0 & 0 & 1 \end{pmatrix} \cdot \begin{pmatrix} 1 & 0 & V_X \\ 0 & 1 & V_Y \\ 0 & 0 & 1 \end{pmatrix} \times \begin{pmatrix} \cos(\theta) & -\sin(\theta) & 0 \\ \sin(\theta) & \cos(\theta) & 0 \\ 0 & 0 & 1 \end{pmatrix} \cdot \begin{pmatrix} 1 & 0 & -V_X \\ 0 & 1 & -V_Y \\ 0 & 0 & 1 \end{pmatrix}. \quad (5)$$

Each point on the mirror is transformed via $P' = \boldsymbol{M} \cdot P$, where the 2D points P and P' are written in homogeneous coordinates, $P = \begin{pmatrix} X \\ Y \\ 1 \end{pmatrix}$ and $P' = \begin{pmatrix} \mathrm{Xy} \\ \mathrm{Yx} \\ 1 \end{pmatrix}$. Substituting $V_\mathrm{X} \rightarrow A_\mathrm{X}$ and $V_\mathrm{Y} \rightarrow A_\mathrm{Y}$, T_X and T_Y as previously described, and noting that the initial probe position is $X = I_\mathrm{x}, Y = I_\mathrm{y}$ and $Z = I_\mathrm{z}$, a cross-coupled motion for each direction in the x–y plane can be obtained by solving for Xy and Yx.

2.2. 3D geometric errors

Similar to the 2D case where a movement along a translation axis also generates a displacement along the perpendicular axis, three plane coupled equations are generated to obtain generic 3D transformations:

$$\begin{aligned} \mathrm{Xy} + \mathrm{Xz} + \mathrm{Yx} + \mathrm{Zx} - 2X_\mathrm{T} - Y_\mathrm{T} - Z_\mathrm{T} = 0, \\ \mathrm{Yz} + \mathrm{Yx} + \mathrm{Zy} + \mathrm{Xy} - X_\mathrm{T} - 2Y_\mathrm{T} - Z_\mathrm{T} = 0, \\ \mathrm{Zx} + \mathrm{Zy} + \mathrm{Xz} + \mathrm{Yz} - X_\mathrm{T} - Y_\mathrm{T} - 2Z_\mathrm{T} = 0, \end{aligned} \tag{6}$$

where, for example, Xy is translation in the x direction with a cross displacement in the y direction, and similarly for other directions. Combining the movement in each plane, the true mirror displacements are obtained self consistently by solving equation 6 for X_T,Y_T and Z_T. The obtained expressions describe corrected displacements in 3D, expressed via measured quantities similar to those in equation 2 but in a much more complex form. As a check, the 3D case reduces to the 2D case for a single plane motion where the solutions are known for a particular set of parameters such as if all the angles are zero (rotation and alignment). In that case, the corrected displacements, i.e. i_T, reduce to the interferometric measurement values, M_i, where $i = X, Y, Z$.

3. Application of local geometric error corrections

Experimentally measuring variables which contribute to measurement errors makes error corrections possible [9]. These additional channels of information together with an appropriate model, can be utilised at each measurement point to correct errors and estimate realistic uncertainties [10]. In the particular case of geometric errors, measurements of parasitic stage rotations by the angular interferometers carry the necessary information about the errors. Combining this with an appropriate model which relates the stage motion and the interferometric measurement configuration through known geometric parameters such as the dimensions of the movable mirror, is sufficient to determine and correct for the local geometric errors. The local character of the method ensures that the error at each subsequent measurement step can be evaluated and that the coordinates of the measurement points can be corrected and complemented by calculation of the corresponding local uncertainties arising from the geometric errors. Applying the derived model from the previous section, to express the true displacement of the mirror via measurable quantities, a stepwise error correction of the measurement data can be performed. The corresponding uncertainties are calculated through standard error propagation methods (equation 1). Typical input values with corresponding uncertainties for parameters used in the local correction model determined prior to a measurement are listed in table 1.

Table 1. Measured values and estimated uncertainties used as input parameters in the local geometrical model for a typical measurement. θ-angle between the movable and reference mirrors.

Measurement constants	Value	Uncertainty
I_x[mm]	38.0	0.08
I_y[mm]	38.0	0.08
I_z[mm]	29.2	0.08
$\theta_\mathrm{x,y,z}$[μrad]	133	5
α, β, γ[μrad]	75	5
$TIO_\mathrm{x,y,z}$[μm]	0	30

Figure 3(a) illustrates an application of the local GEC method for a typical mSPM scan of a height calibration artefact[3]. The local GECs are visualised with black vectors and corresponding uncertainties with red spheres. Both thebreak vector and uncertainty components are calculated for each measurement step of the mSPM. The 3D features of the measured structure are clearly recognizable. With this sequential approach, the steps are determined by the scan speed and resolution of the angular interferometers. A zoom into one of the artifact's step feature is shown in figure 3(b). The local correction vectors do not show a clear orientation trends while the uncertainties tend to be slightly larger at the valley and on the plateau of the step compared with other measuring locations. For quantifiable results it is helpful to visualise both local error correction and corresponding uncertainty distributions for all the three displacement axes as in figure 4(a) and (b). The correction errors follow the normal distribution for each of the directions with 95% of the correction vector components ranging between ±1 nm. The local uncertainty distribution follows a log-normal distribution reasonably well, with a mean value of 0.04 nm. The local GEC uncertainties are dominated by the uncertainty of the Abbé error offsets, ±110 μm.

4. Local versus global geometric error correction methods

The common approach for complex dimensional measuring instruments such as a coordinate measuring machine (CMM) is to globally evaluate 21 geometric errors [6]. These errors are determined by measuring various geometric parameters over the dynamic range of the instrument. The approach of using a global GEC method where specific experimental

[3] The artefact is TGQ1 calibration grating from the NT-MDT. The grating specification are described in *AFM Probes & Accessories Catalogue—NT-MDT* www.ntmdt-tips.com/data/media/images/nt_mdt_afm_probes_2012.pdf (Accessed: 17 December 2019).

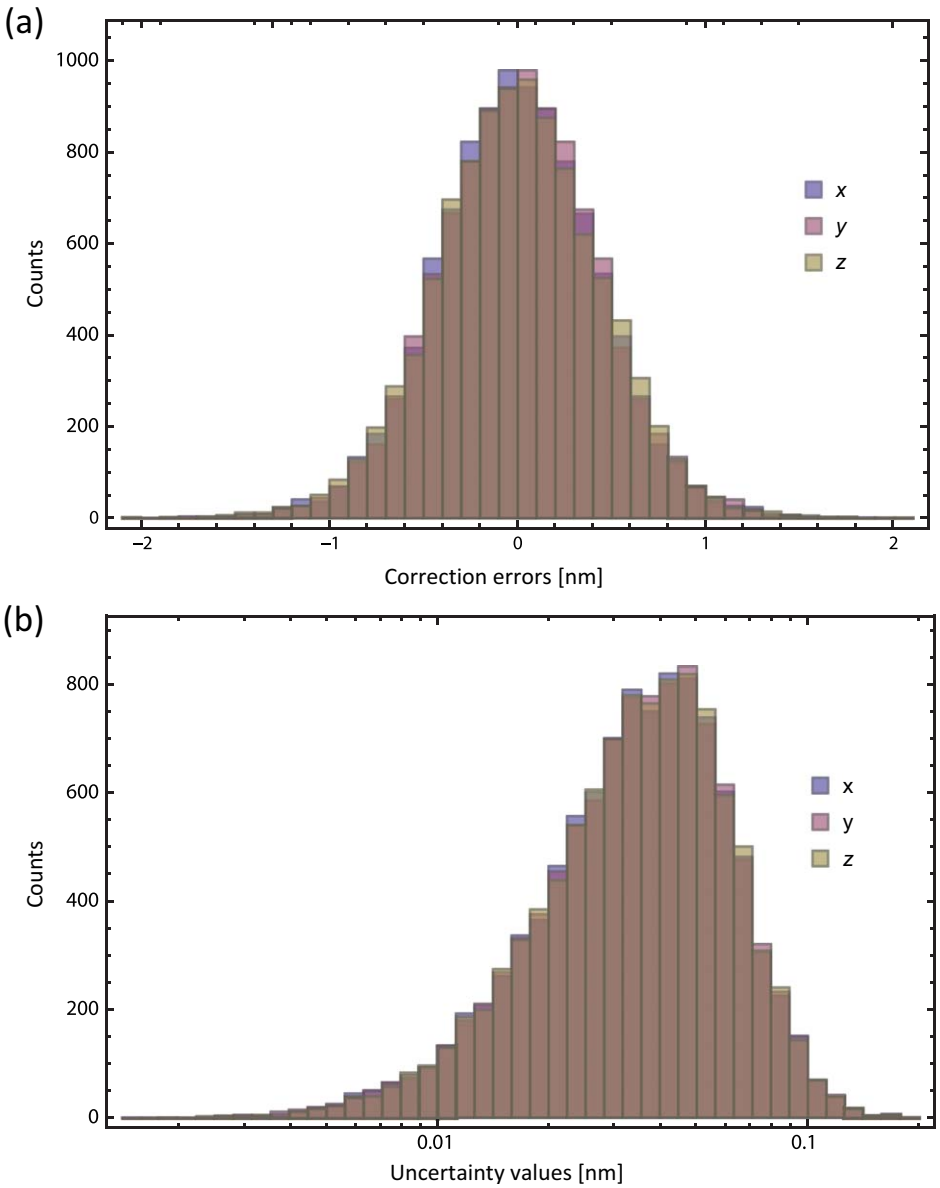

Figure 4. Distributions of (a) the local error correction vector components, and (b) the local uncertainty components. On both histograms every 364th point is shown from the acquired data set.

procedures are developed to separate each type of error, can be cumbersome, impractical and ineffective due to high requirements on repeatability. For example, measuring nine parasitic rotations due to three translational displacements on one hand requires regular calibrations for each set of measurements, and on the other hand overestimates uncertainties by inherently demanding that the largest global uncertainty value represents the overall uncertainty. A simple estimate based on the stage's specified parasitic rotations with known Abbé offsets shows that the Abbé errors are the largest cumulative contribution to the uncertainty budget of the instrument for large displacements. While some manufacturers of scanning stages provide global values for the parasitic rotations $\Delta\phi$ in the linear form $\Delta\phi = c_\mathrm{r} \cdot \Delta x$, where c_r is the sensitivity coefficient and Δx is the displacement, these values can be misleading and may not provide an accurate estimate of the stage motion. This is illustrated in figure 5, where the roll angle is measured for x axis motion in the mSPM. From the measurement data, it is evident that the assumed linearity of the stage rotation versus the displacement is merely a convenient approximation. In addition, the spread of the angle values varies dramatically with the displacement where the ratio of measured data variations at the scan limits is ≈ 6, as can be deduced from differential roll angle values shown in the inset of figure 5.

A qualitative comparison between local and global GEC methods can be obtained from scaling of the corresponding uncertainties on a step parameter, n. Let us consider a simple case where the functional form of a dependent variable (measurand), m, is given by a single polynomial term with a power law dependence on a measurement variable, d. For example, it can be the dependence of a parasitic rotation angle, m, on a

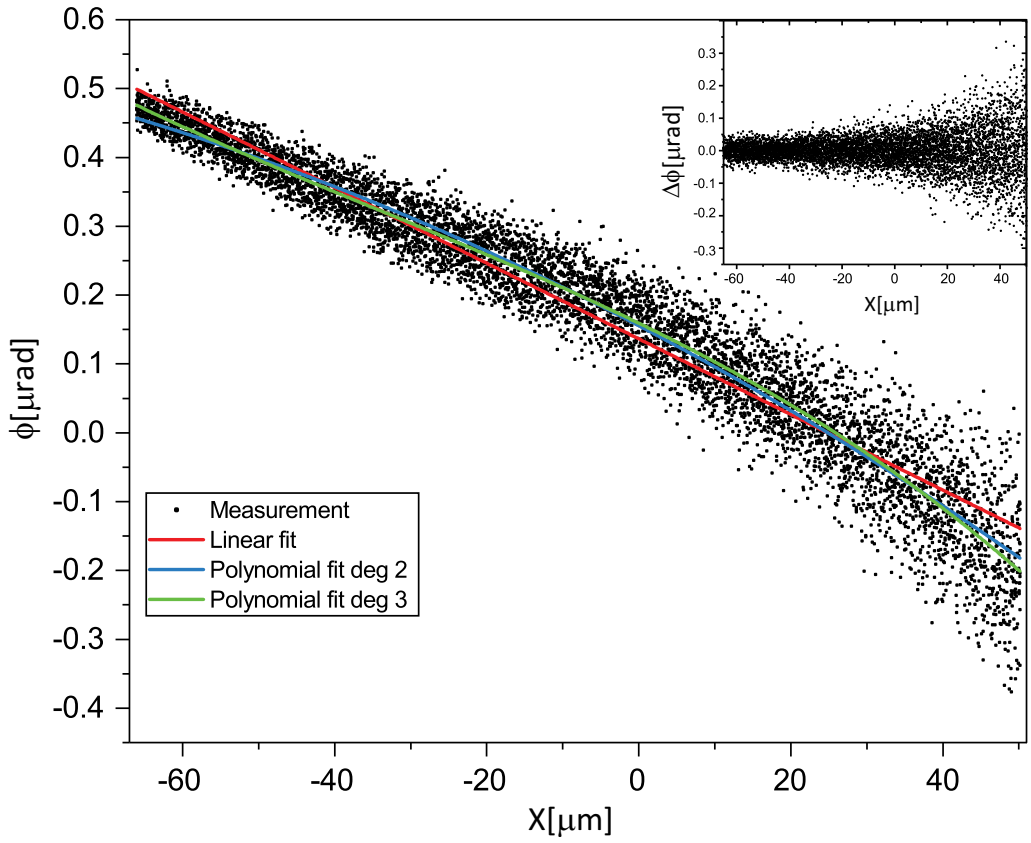

Figure 5. Position dependence of the roll angle, ϕ, for x–axis displacement. Measurements (symbols) and fits using 1st (red), 2nd (green), 3rd (blue) order polynomials. Inset: Plot of the subsequent angle differences.

displacement d, $m = k \times d^r$, where k is the constant of proportionality, r is the exponent. The comparison criteria between the local and global methods will be the total measurand's uncertainty for a given displacement.

For the local method, substituting $d \to \left(\frac{d}{n}\right)$ models the local character of the method where the displacement is subdivided into n steps, for a total of $n+1$ measurement points. The uncertainty of the measurand can be found using equation 1, where the sensitivity coefficient has the form $c = r \times k/n^r \times d^{(r-1)}$, followed by summation of n local error terms, ε, within a step d/n. For the step error ε we consider two possibilities of interpolation in each segment d/n:

$$\begin{aligned} &\epsilon = \epsilon_0, \quad \text{for zero order interpolation}(L0) \\ &\epsilon = c_\epsilon \int_0^{d/n} d\epsilon = c_\epsilon d/n, \quad \text{for linear interpolation}(L1), \end{aligned} \tag{7}$$

where c_ϵ, is the step error proportionality constant. The total local uncertainty scales as $u_{L0} = \sqrt{\sum_{i=1}^{n}(c\epsilon_0)^2} = c\epsilon_0\sqrt{n} \propto \epsilon_0 \times d^{(r-1)}/n^{r-1/2}$ for the zero order interpolation, and as $u_{L1} \propto d^r/n^{r+1/2}$ for the first order interpolation.

The global uncertainty is strictly speaking deduced from a fit to the measured points assuming a functional dependence between m and d. For a generic power law, coefficients are varied to obtain a best fit, where the uncertainty of the coefficients scales as $1/\sqrt{n}$. Since we are interested only in scaling, the global cumulative uncertainty has a scaling dependence of $u_G \propto 1/\sqrt{n} \times d^r$. Hence, the scaling ratios of the local versus global cumulative uncertainties are

$$\begin{aligned} &u_{L0}/u_G \propto \frac{1}{d\sqrt{n}^{(r-1)}}, \quad \text{zero order interpolation}, \\ &u_{L1}/u_G \propto \frac{1}{n^r}, \quad \text{for linear interpolation}. \end{aligned} \tag{8}$$

For the first three polynomial exponents, $r = 0, 1, 2$, the total uncertainty ratios of the linear error interpolation are displacement independent and have step number dependences $\left\{1, \frac{1}{n}, \frac{1}{n^2}\right\}$ as shown in figure 6(a). The local vs. global uncertainty ratio is constant for $r = 0$, while for $r > 0$ scaling of the ratio decreases with the step number. For the zero order error interpolation, the ratio is inversely proportional to displacement d, indicating again the superiority of the local method. The step dependence is weaker than for the linear error interpolation, and if the displacement d is constant, the total uncertainty ratio is independent of the step numbers for the linear step accumulation ($r = 1$), and as the exponent increases the local uncertainty decreases for the same number of steps. Also, the errors are diminishing as the number of steps increases while for a single step ($n = 1$) the uncertainties for both methods are the same as expected. Interestingly, for the linear interpolation case when the power dependence is not existent ($r = 0$), the global approach tends to have a smaller total uncertainty with scaling $\sqrt{n}$ for the ratio between local and global methods. In this case, a segmentation makes little sense

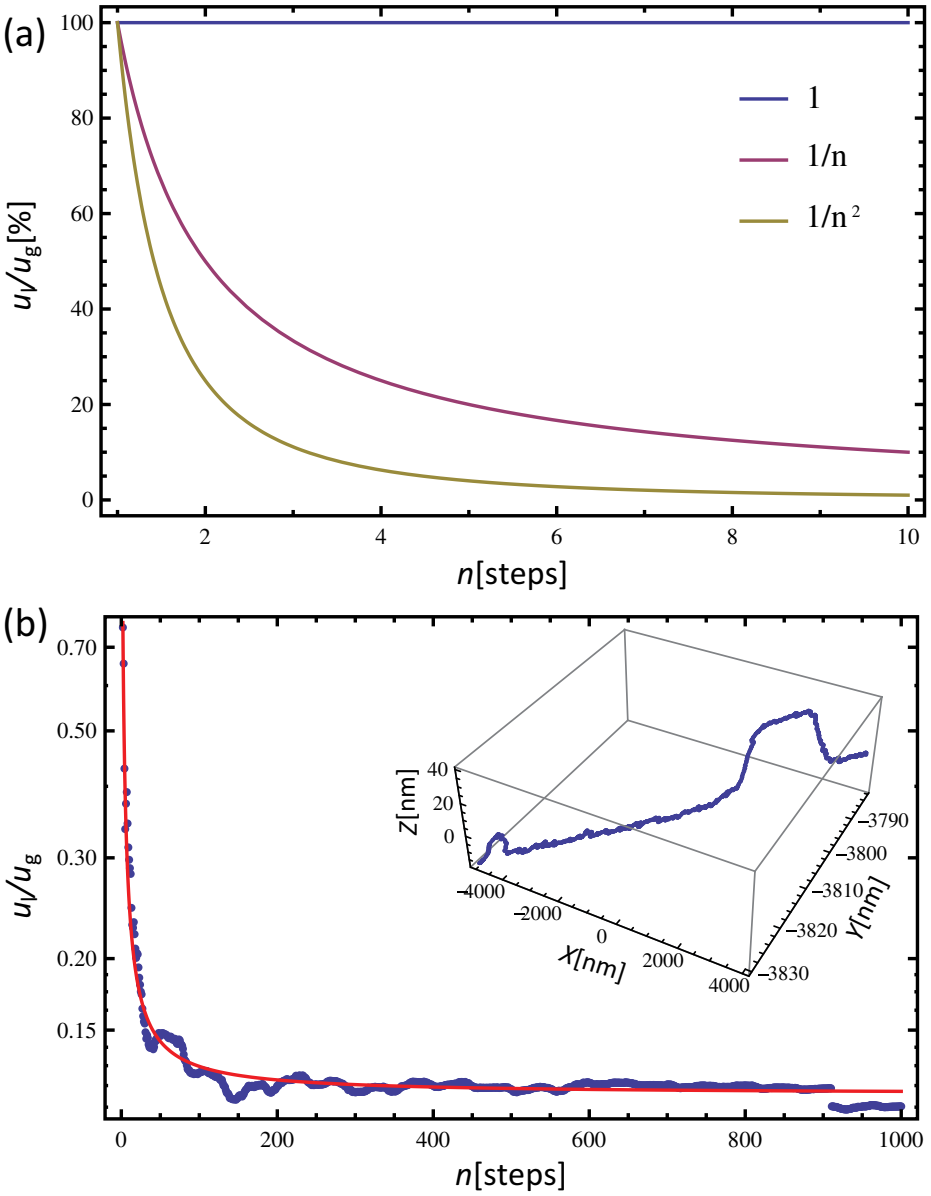

Figure 6. Scaling dependence of the local and global GEC method uncertainty ratio as a function of the number of measurement steps. (a) The uncertainty ratio versus step number for linear interpolation of the step error (equation 8). (b) The cumulative uncertainty ratio for measurement data (symbols) taken by the mSPM, with a line of best fit, ($u_{L1}/u_G = 0.012 + 1.44/n$), for the linear interpolation as per equation 8. Inset: The measurement points for a linear mSPM scan.

since it unnecessarily exaggerates displacement errors by data oversampling, leading to an overestimate of the corresponding total local uncertainty.

In a realistic case, a functional form of all the interrelationships between variables contributing to uncertainties may not be known or may be extremely complex. Take as an example a linear mSPM trace as in the inset of figure 6(b). The trace contains a large displacement in the x direction with cross displacement in y and a sample feature displacement in the z direction in the MRS. To make the analysis more transparent let us look at the one-dimensional case of comparing the local and global uncertainty ratio for an x direction displacement, where the probe shape uncertainty was not included in the analysis. After applying the local GECs, the corresponding uncertainties can be calculated from the general displacement expressions for X_T, Y_T and Z_T obtained by solving equation 6. A total uncertainty is obtained by summing the local uncertainty contributions in quadrature for a given step range. The global GEC method will lead to a cumulative uncertainty which scales with distance, $u_G = d \times \epsilon_{max}/\sqrt{n}$. The ratio of the uncertainties (symbols) is plotted versus the number of steps in figure 6(b). The ratio drops quickly after 10 steps, having a pseudo-oscillatory nature for larger numbers of measurement steps, progressively settling with a further increase in step numbers. These variations are due to the contributions from the other two axes of motion, which are small but not negligible, and can have a dramatic influence on the continuity of data, visible in figure 6(b) as a sharp drop around $n = 900$.

The ratio data can be fitted to the step scaling functions as in equation 8. The line in figure 6(b) shows a best fit to the first two terms of the linear error interpolation.

5. Conclusion

The GEC method applied to measurement data obtained with the NMIA mSPM leads to a reduction of positional errors up to 10 nm. The local GEC method can achieve a significant reduction in the uncertainty of displacement measurements bringing it well into the subnanometre range. This method generally outperforms the global GEC method, as demonstrated through a derived scaling dependence of the cumulative uncertainty on the number of measurement steps. For a typical data set, the local method reduces the total displacement uncertainty by at least 60% compared to the global method. A further advantage of the local GEC method is its application when a localised feature of a sample has to be accurately measured. Even in the case of an ensemble measurement, such as measuring a group of nanoparticles, the local method is more accurate due to the common practice of determining nanoparticle height [11] from the relative height of the highest pixel relative to a reference plane, which is a single measurement point. Universally, the local GEC method does not rely on repeatability, hence it is an *in situ* method where dynamic properties of a scan, such as the direction and speed, are reflected merely in different correction vectors and uncertainties. The local method is highly suitable for application in conjunction with our laser interferometry system. Since our interferometric system bandwidth (1 kHz) is substantially higher than a typical stage scanning line speed (< 10 Hz), the potential number of acquired points is always sufficiently large to justify application of the local GEC method, while at the same time maintaining sufficiently small step size between subsequent points such that linear error interpolation is appropriate. The above considerations suggest that the local GEC method should be applied whenever possible, due to its characteristic ability to exploit the knowledge of both the measurement process and the measurement system, without influencing and hence, compromising performance and integrity of the measurements.

Acknowledgment

The authors acknowledge help from Patrick Gilfillan, Chris Freund, Malcolm Gray and Malcolm Lawn.

ORCID iD

Bakir Babic https://orcid.org/0000-0002-7869-1898

References

[1] Cory D G, Price M D, Maas W, Knill E, Laflamme R, Zurek W H and Somaroo S S 1998 Experimental quantum error correction *Phys. Rev. Lett.* **81** 2152
[2] Serban R, Koon W S, Lo M W, Marsden J E, Petzold L R, Ross S D and Wilson R S 2002 Halo orbit mission correction maneuvers using optimal control *Automatica* **38** 571
[3] Babic B, Freund C, Coleman V A and Herrmann J 2018 A metrological scanning probe microscope for accurate length measurements at the nanoscale *Australian Physics* **55** 12
[4] Babic B, Freund C H, Herrmann J, Lawn M A and Miles J 2011 *Journal of Micro/Nanolithography, MEMS, and MOEMS* **11** 1
[5] Bobroff N 1993 Critical alignments in plane mirror interferometry *Precision Engineering* **15** 33
[6] Hocken J and Pereira P H (ed) 2011 *Coordinate Measuring Machines and Systems* 2nd edn pp 573 (CRC Press: Boca Raton, FL)
[7] Bentley R E *Uncertainty in Measurement: The ISO Guide* (National Measurement Institute) pp 29
[8] Davis T 2019 *Homogeneous Coordinates and Computer Graphics* www.geometer.org/mathcircles/cghomogen.pdf (Accessed: 25 July 2019)
[9] Leach R 2010 *Fundamental principles of engineering Nanometrology*, 1st edn (Elsevier: Amsterdam) pp 269
[10] Klapetek P, Nečas D, Campbellová A, Yacoot A and Koenders L 2011 Methods for determining and processing 3D errors and uncertainties for AFM data analysis *Meas. Sci. Technol.* **22** 025501
[11] Babic B, Lawn M A, Coleman V A, Jämting Å K and Herrmann J 2016 Minimising the effect of nanoparticle deformation in intermittent contact amplitude modulation atomic force microscopy measurements *J. Appl. Phys.* **119** 214307